analytical chemistry

pubs.acs.org/ac Article

High-Throughput Colorimetric Analysis of Nanoparticle–Protein Interactions Based on the Enzyme-Mimic Properties of Nanoparticles

Mengyao Wen, Juanmin Li, Wencheng Zhong, Jie Xu, Shaohua Qu, Hui Wei, and Li Shang*

Cite This: *Anal. Chem.* 2022, 94, 8783–8791 Read Online

ACCESS | Metrics & More | Article Recommendations | Supporting Information

ABSTRACT: While an in-depth understanding of the biological behavior of engineered nanoparticles (NPs) is of great importance for their various applications, it remains challenging to quantitatively characterize NP–protein interactions in a simple and high-throughput manner. In the present work, we propose a new, colorimetric approach capable of quantitatively analyzing the adsorption of proteins onto the surface of NPs by their distinct peroxidase-mimic properties. Taking cationic AuNPs as an example, we demonstrate that this colorimetric method is capable of evaluating NP–protein interactions in a simple and high-throughput manner in multiwell plates. Important binding parameters (e.g., the binding affinity) of three different serum proteins (bovine serum albumin, transferrin, and lysozyme) as well as human serum to AuNPs with three different sizes (average diameters of 5, 10, and 15 nm) have been obtained. Based on a quantitative analysis of NP–protein interactions, we observe that the binding affinity and the inhibition efficiency of the nanozyme activity of AuNPs are strongly affected by the characteristics of proteins as well as the sizes of NPs. These results illustrate the great potential of the present colorimetric method as a simple, low-cost, and high-throughput platform for quantitatively investigating NP–protein interactions.

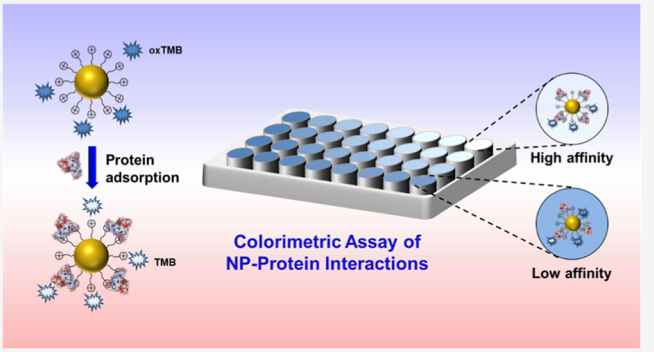

1. INTRODUCTION

Over the past decades, engineered nanomaterials have been widely applied in biomedical fields, such as drug delivery, bioimaging, and disease diagnosis.[1−5] However, when nanomaterials enter a biological environment, serum proteins inevitably adsorb to their surfaces to form a "protein corona" immediately.[6] In most cases, the protein corona alters the physicochemical properties of nanomaterials,[7] determining their biological behaviors in terms of targeting ability,[8] immune response,[9] cellular internalization,[10] and cytotoxicity.[11] Therefore, an in-depth understanding of nanomaterial–protein interactions is of great importance for designing safe and effective functionalized nanomaterials and advancing their clinic applications.[12,13] Despite the great efforts devoted to understanding nano–bio interactions in the past years,[14,15] a complete picture depicting the protein adsorption behaviors onto the surface of nanomaterials has not been achieved yet, which is mainly due to the versatile types of nanomaterials as well as the lack of efficient and generable characterization tools.

Until now, researchers have developed different biophysical techniques to elucidate mechanistic aspects of nanomaterial–protein interactions. For example, gel electrophoresis,[16] mass spectrometry,[17] and synchrotron radiation X-ray absorption spectroscopy[18] can provide ex situ information of protein–nanoparticle (NP) complexes separated from unbound proteins, whereas in situ methods such as fluorescence quenching,[19,20] fluorescence correlation spectroscopy,[21] isothermal titration calorimetry,[22] and nuclear magnetic resonance[23] can directly monitor the protein adsorption in the biological environments. However, these methods are normally incapable of achieving high-throughput quantitative analysis of the protein corona due to the complexity of operation or vulnerability to environmental interference, which greatly limits the efficiency of extracting important information from NP–protein interactions and the reliability of experimental results from different measurements. Therefore, it is necessary and important to develop new analytical tools to quantitatively characterize NP–protein interactions in a simple and high-throughput manner.

Recent studies revealed that a wide variety of engineered NPs exhibit interesting catalytic characteristics that mimic the

Received: April 13, 2022
Accepted: May 27, 2022
Published: June 9, 2022

https://doi.org/10.1021/acs.analchem.2c01618
Anal. Chem. 2022, 94, 8783–8791

functions of natural enzymes.[24−27] For example, similar to horseradish peroxidase (HRP), many inorganic NPs, such as Fe_3O_4 NPs,[28] AuNPs,[29] metal nanoclusters,[30] and graphene oxides,[31] can oxidize colorless TMB (3,3′,5,5′-tetramethylbenzidine) to a colored product (oxTMB) in the presence of H_2O_2, leading to a remarkable absorbance change. Importantly, the intrinsic peroxidase-like activity of these NPs is strongly influenced by their surface environment,[32−35] and the adsorption of additional substances from the solution (e.g., small molecules and biomolecules) will likely affect the catalytic efficiency of the colorimetric reaction. Consequently, the absorbance of the solution shows changes that can reflect such adsorption events. Therefore, we envision that the adsorption of proteins onto the surface of these NPs can be monitored by the peroxidase-based colorimetric method. Particularly, the peroxidase-based colorimetric method can be easily integrated with microplate readers, making it possible to achieve the high-throughput quantitative measurement, i.e., characterizing multiple NP−protein samples simultaneously. Cationic NPs possess great potential in biomedicine due to their easy binding to biomolecules and favorable cellular internalization,[36−38] but the study of their interactions with biological systems (e.g., protein adsorption) remains limited. As an example, we chose AuNPs, one of the most commonly studied nanomaterials,[39−41] as the model cationic NPs, and investigated their interactions with serum proteins via the proposed colorimetric method. Using a microplate reader to measure the absorbance change of the solution, we demonstrated the feasibility of in situ evaluating the protein adsorption process in a simple and high-throughput manner (Scheme 1). Important binding parameters (e.g., the binding affinity) of three different serum proteins to AuNPs with three different sizes can be easily obtained. As a result, the influence of protein characteristics and particle size on NP−protein interactions has been elucidated by this colorimetric method.

Scheme 1. Schematic Illustration of Quantitative Analysis of Protein Adsorption on the Surface of AuNPs by the Colorimetric Method

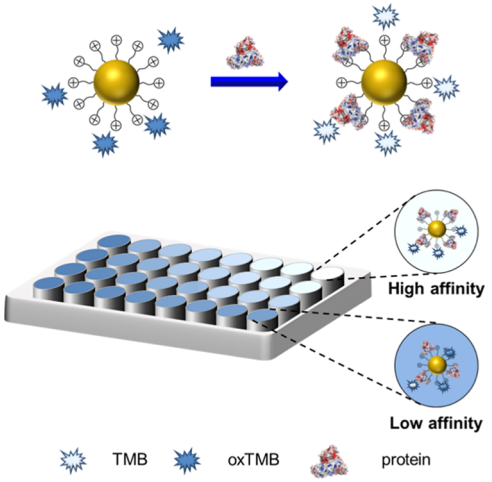

2. EXPERIMENTAL SECTION

2.1. Preparation of AuNPs. (11-Mercaptoundecyl)-*N*,*N*,*N*-trimethylammonium bromide (MUTAB) was chosen as a ligand to synthesize cationic MUTAB−AuNPs via a two-step phase transfer protocol modified from the previous report.[42] Briefly, citrate−AuNPs with a diameter of 5 nm were prepared using $NaBH_4$ as a reducing agent,[43] while citrate−AuNPs with diameters of 10 and 15 nm were synthesized using the Frens method.[44] Water-soluble citrate ligands on the surface of AuNPs were exchanged with octadecylamine (ODA) ligands, yielding oil-soluble ODA−AuNPs. Then, MUTAB was added to the solution of ODA−AuNPs, which resulted in water-soluble MUTAB−AuNPs owing due to strong Au−thiolate interactions. Details on the synthesis and characterization of citrate−AuNPs and MUTAB−AuNPs are provided in the Supporting Information.

2.2. Absorption Measurement of Bovine Serum Albumin (BSA)−AuNP Interactions. To minimize the effect on the structure and function of proteins, phosphate-buffered saline (PBS, 10 mM, pH 7.0) was used as a medium to study the peroxidase-like activity of MUTAB−AuNPs in the absence or the presence of proteins at 37 °C. First, the concentration of TMB and H_2O_2 was optimized according to the absorbance of 652 nm (oxidized TMB). MUTAB−AuNPs (50 μM Au concentration) were incubated with varying bovine serum albumin (BSA) concentrations (0.0001−2 μM) in PBS (10 mM, pH 7.0) for 60 min, and then optimized concentrations of TMB (4 mM) and H_2O_2 (1.2%) were added. After incubation at 37 °C for 40 min, UV−vis absorption spectra (500−800 nm) were measured, and the binding affinity was assessed by the quantitative analysis of the BSA concentration dependence of the absorbance values at 652 nm ($A_{652\,nm}$) with the modified Hill equation[45−47]

$$\frac{E}{E_{max}} = \frac{1}{1 + (K_D'/C_{protein})^n} \quad (1)$$

$$E = (A_0 - A)/A_0 \quad (2)$$

where A and A_0 are the absorbances of the solution at 652 nm in the presence and the absence of protein, respectively, E is the suppression efficiency of AuNPs' peroxidase-like activity, E_{max} denotes the maximum value of E, K_D' represents the apparent equilibrium dissociation coefficient of NP−protein interactions, $C_{protein}$ denotes the protein concentration, and n is the Hill coefficient.

2.3. Quantitative Analysis of Protein−AuNP Interactions Using a Microplate Reader. Generally, a multiwell plate was used to analyze the interaction of AuNPs with apotransferrin (Tf), lysozyme (Lyz), and serum. MUTAB−AuNPs (50 μM Au concentration) were incubated with different concentrations of protein at 37 °C for 60 min in a PBS solution (10 mM, pH 7.0). Subsequently, 40 μL of a solution containing 20 mM TMB and 6.0% H_2O_2 was added and incubated at 37 °C for 40 min. Then, the absorbance of the solution at 652 nm was measured with the microplate reader. Interactions between proteins and AuNPs of different sizes were studied with similar strategies as described above.

3. RESULTS AND DISCUSSION

3.1. Synthesis and Characterization of MUTAB−AuNPs. Cationic NPs possess great potential in various fields, such as drug delivery, antimicrobial, and biosensing,[38,48] but their interactions with biological systems (e.g., protein adsorption) remain poorly exploited yet compared with their anionic counterparts. Therefore, we chose cationic AuNPs as the model systems in the present study. Herein, cationic AuNPs were synthesized by a two-step ligand exchange

https://doi.org/10.1021/acs.analchem.2c01618
Anal. Chem. 2022, 94, 8783−8791

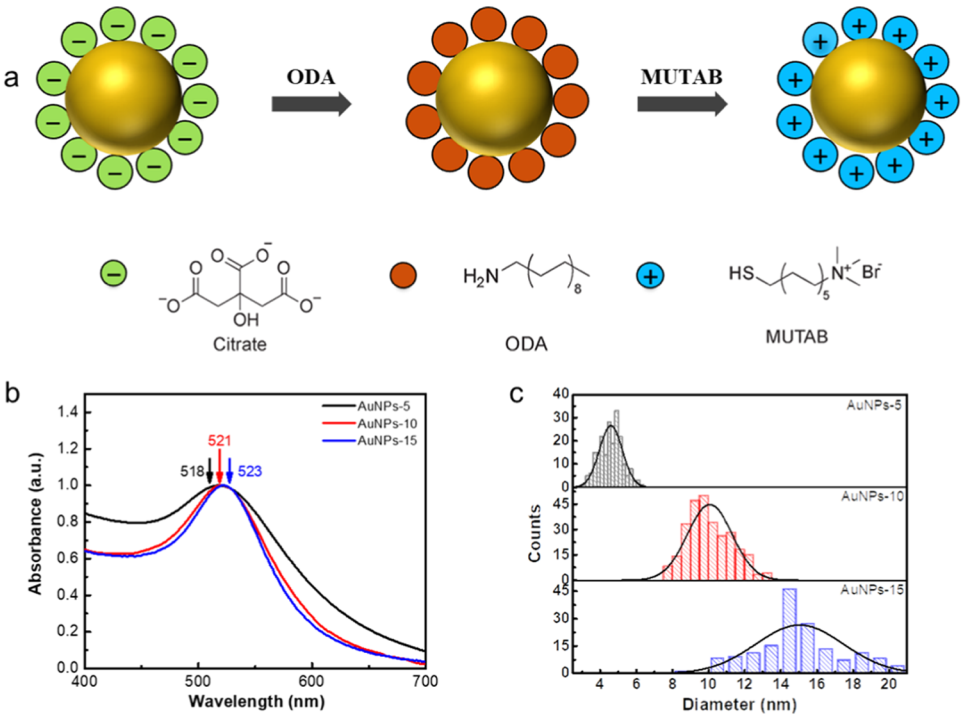

d

AuNPs	SPR peak (nm)	TEM diameter (nm)	Hydrodynamic diameter (nm)	Zeta potential (mV)
AuNPs-5	518	4.6±0.6	8.0±0.2	+38.9±3.2
AuNPs-10	521	10.1±1.2	13.0±0.3	+38.6±0.7
AuNPs-15	523	15.0±2.4	18.1±0.3	+41.8±1.7

Figure 1. (a) Schematic illustration of synthesizing MUTAB−AuNPs via a two-step ligand exchange strategy. Absorption spectra (b) and the size histogram (c) of MUTAB−AuNPs based on TEM images. (d) Table of physicochemical characterization of MUTAB−AuNPs of different sizes.

strategy modified from the previous report (Figure 1a).[42] Citrate−AuNPs with negative surface charges were first prepared and octadecylamine (ODA) was employed as an amine-capped intermediate before the ligand exchange with positively charged ligands (MUTAB) to avoid the occurrence of irreversible aggregation. As shown in Figure 1b, MUTAB−AuNPs of different sizes exhibit apparent surface plasmon resonance (SPR) absorption bands in the range of 518−523 nm. Transmission electron microscopy (TEM) characterization (Figure S1) revealed that MUTAB−AuNPs are well dispersed with a core size of 4.6 ± 0.6 nm (denoted as AuNPs-5), 10.1 ± 1.2 nm (denoted as AuNPs-10), and 15.0 ± 2.4 nm (denoted as AuNPs-15), respectively (Figure 1c). As expected, the hydrodynamic diameter of these MUTAB−AuNPs is slightly larger than their core size due to the contribution of surface ligands and hydration layers. ζ-Potential of all three types of MUTAB−AuNPs was greater than +30 mV, indicating good colloidal stability of these cationic AuNPs. The above characterization showed that these MUTAB−AuNPs exhibit abundant positive surface charges, good size uniformity, and colloidal stability, which make them promising for the subsequent protein adsorption studies.

3.2. Quantitative Analysis of AuNP−Protein Interactions by Colorimetry. To evaluate the feasibility of characterizing NP−protein interactions by the peroxidase-mimic colorimetric reaction, we first studied interactions of AuNPs-5 with bovine serum albumin (BSA), the most commonly adopted protein system. As shown in Figure 2a, AuNPs-5 (average diameter of 4.6 nm) indeed exhibits peroxidase-like catalytic features, which can oxidize the substrate TMB into a blue product with the maximum absorbance at 652 nm in the presence of H_2O_2. Control experiments showed that both AuNPs and H_2O_2 are necessary for the oxidation of TMB. The concentration of TMB and H_2O_2 was optimized to yield the largest colorimetric changes, and 4 mM TMB and 1.2% H_2O_2 were chosen (Figure S2). To best mimic the physiological condition of NP−protein interactions, the colorimetric experiments were all performed in PBS with a pH of 7.0 at 37 °C.

As shown in Figure 2b, with increasing the BSA concentration in the solution of AuNPs, a gradual decrease in the absorbance in the absorption spectra was observed. This fact suggests that the peroxidase-like catalytic activity of MUTAB−AuNPs was weakened in the presence of BSA, likely due to the occurrence of protein adsorption that inhibits the proximity of the substrate to the surface of AuNPs.[49,50] We note that in one previous study, the nanozyme activity of iron oxide NPs is increased upon protein adsorption,[51] which is different from the present case. It is likely that the features of the formed protein corona, such as the protein orientation and the corona composition, may pose a significant role in the catalytic process. The dependence of the absorbance at 652 nm

https://doi.org/10.1021/acs.analchem.2c01618
Anal. Chem. 2022, 94, 8783−8791

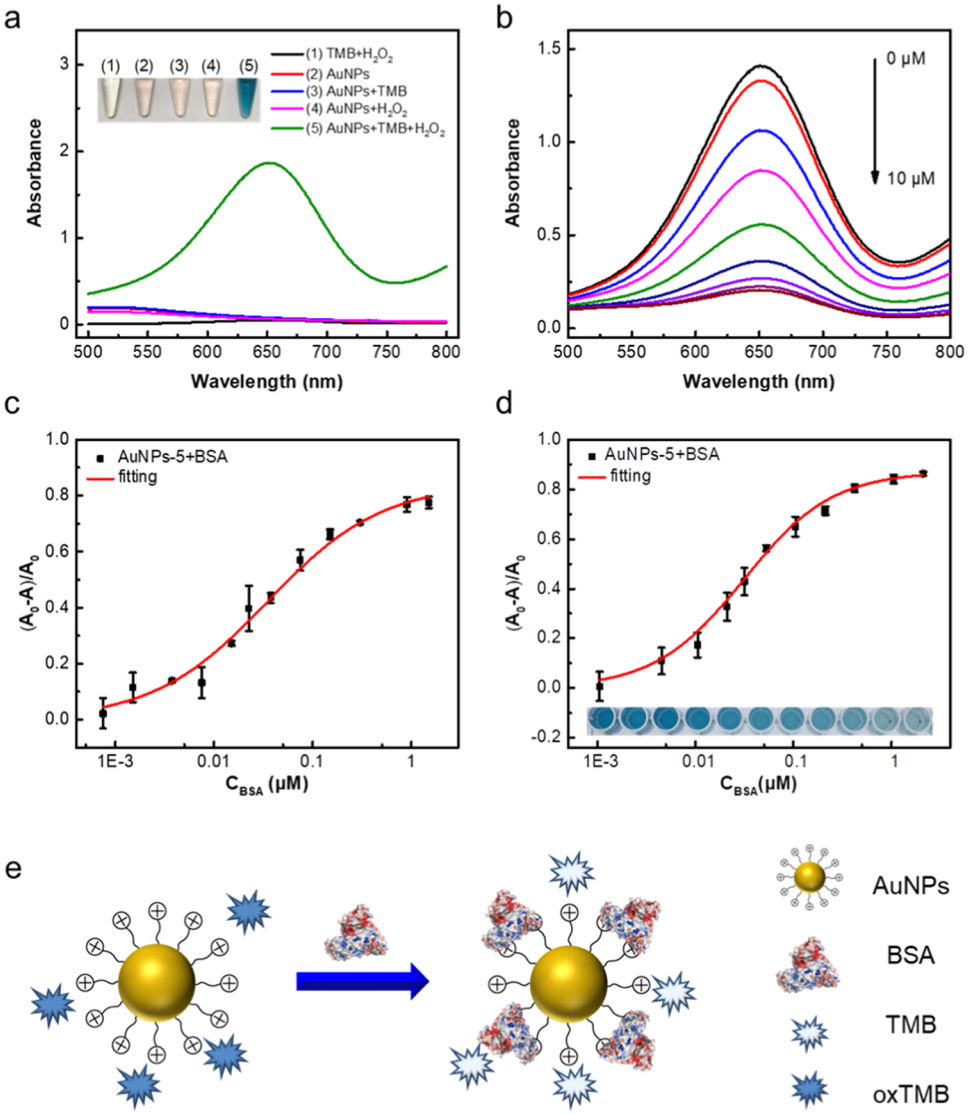

Figure 2. (a) Peroxidase-like activity of AuNPs-5. (b) UV−vis absorption spectra of AuNPs-5 with BSA in the TMB−H_2O_2 system. Fitting of the absorbance data that were obtained by the spectrophotometer (c) and the microplate reader (d) with the Hill equation (red line). (e) Schematic diagram of interactions between AuNPs-5 and BSA. A and A_0 are the absorbances of the solution at 652 nm in the presence and the absence of protein, respectively.

on the protein concentration can be further quantitatively analyzed via the modified Hill equation (see the Experimental Section), which can yield parameters characterizing the binding affinity between AuNPs and protein. As shown in Figure 2c, upon fitting the results with eq 1, an excellent agreement could be obtained, which yielded $K_D' = (3.5 \pm 0.4) \times 10^{-8}$ M. The maximum efficiency, $E_{max} = 0.84 \pm 0.03$, suggests a high suppression effect of BSA adsorption on the peroxidase-mimicking activity of AuNPs. It is worth noting that this K_D' value is much smaller than that of BSA binding to AuNPs with negative charges, ∼a 100-fold increase in the binding affinity.[47,52,53] Meanwhile, a similar strong affinity was observed for cationic metal-oxide NPs interacting with HSA[54] or cationic protein adsorption onto anionic AuNPs[55] that were measured by surface plasmon resonance or second harmonic light scattering techniques, indicating that the high NP−protein affinity is largely governed by electrostatic interactions.

To evaluate the reliability of the present colorimetric method for characterizing NP−protein interactions, we next investigated whether the presence of TMB and H_2O_2 in the solution affects the conformation of the protein and their adsorption behaviors with NPs. Our results showed that the circular dichroism spectra of BSA remain almost unchanged in the presence of either TMB or H_2O_2 (Figure S3), indicating that the secondary conformation of BSA was not affected by TMB or H_2O_2 in the measurement solution. Moreover, the absorption spectra of the BSA−AuNP solution also remained unaltered upon further adding TMB or H_2O_2 (Figure S4), suggesting that TMB and H_2O_2 had negligible influence on interactions between AuNPs and BSA. Previously, researchers reported a few cases of nanozyme inactivation due to NP aggregation, competitive binding to NPs' surfaces, and inhibition of the generation of reactive oxygen species (ROS) during the catalytic process.[32,56−58] Herein, no aggregation of AuNPs was observed in the measurement, as supported by the excellent colloidal stability in the mixture solution (Figure S4). On the other hand, using terephthalic acid as a fluorescence probe of a hydroxyl radical (•OH), we

https://doi.org/10.1021/acs.analchem.2c01618
Anal. Chem. 2022, 94, 8783−8791

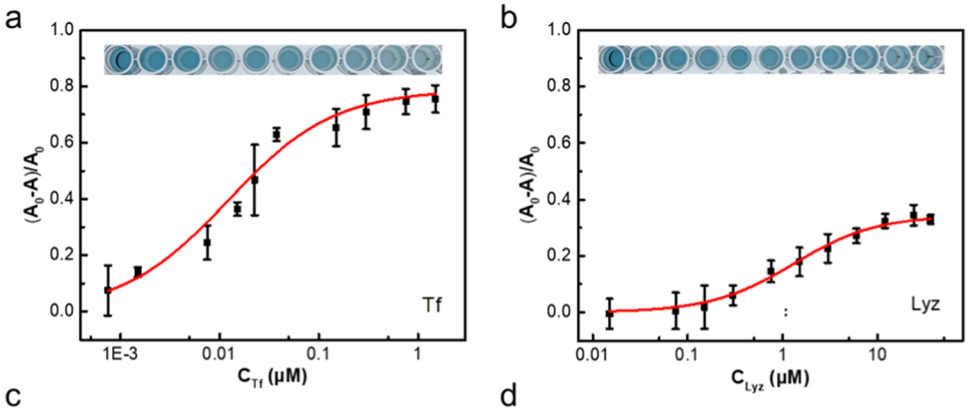

Protein	BSA	Tf	Lyz
MW (kD)	66.4	88.0	14.7
pI	4.7	5.9	11.3
D_H(nm)	5.1	6.6	3.1
ζ (mV)	-7.3	-16.5	+7.0
Structure			

Figure 3. Peroxidase-like activity of AuNPs-5 at different protein concentrations in the TMB−H_2O_2 system: Tf (a), Lyz (b), and serum (d). Red lines represent the fitting results to the Hill equation. (c) Structure and properties of three serum proteins in the present study. A and A_0 are the absorbances of the solution at 652 nm in the presence and the absence of protein, respectively. Red and blue colors in the protein structure correspond to negatively and positively charged patches, respectively, calculated by PyMOL software.

found that the level of generated •OH for AuNPs-5 was not affected upon the BSA adsorption (Figure S5).

Based on the above facts, we infer that the adsorption of protein molecules on the surface of AuNPs will form a "corona" layer, which then effectively shields the surface of AuNPs from the substrate (Figure 2e). As a result, the peroxidase-like catalytic activity of AuNPs was largely suppressed, and the extent of suppression is sensitively reflected by the amount of the colored product, oxTMB. The more proteins adsorbed to the surface of AuNPs, the less oxTMB formed. Therefore, based on these protein adsorption-caused absorbance changes, one can monitor protein−NP interactions in a highly simple and quantitative manner. Furthermore, we also performed the AuNP−BSA binding experiments in the multiwell plates and recorded the absorbance at 652 nm by a microplate reader, from which a similar binding curve was also obtained (Figure 2d). The yielded K_D', $(3.1 \pm 0.3) \times 10^{-8}$ M, is similar to that obtained with a spectrophotometer, which suggests the feasibility of colorimetric measurement of NP−protein interactions by the microplate reader.

3.3. Microplate Reader-Based Colorimetric Analysis of Protein−AuNP Interactions. The above results encouraged us to further exploit interactions between AuNPs and other serum proteins by the microplate reader-based approach. As shown in Figure 3a, similar to BSA, the peroxidase-like activity of AuNPs-5 was significantly decreased in the presence of transferrin (Tf), an important iron-transport protein in the serum. Further quantitative analysis also showed a good fit of the absorbance with the modified Hill equation, which reveals that the binding affinity of Tf to cationic AuNPs-5 (K_D' = (1.2 ± 0.3) × 10^{-8} M) is stronger than that of BSA. In contrast, lysozyme (Lyz) showed an insignificant effect on the enzyme-like activity of AuNPs (Figure 3b), and a much weaker color change was observed in the solution. Consequently, the obtained dissociation coefficient (K_D' = (131 ± 17) × 10^{-8} M) is two orders of magnitude higher than that of BSA, suggesting a rather weak binding affinity of Lyz to cationic AuNPs. These results indicate that the peroxidase-like catalytic activity of AuNPs will be suppressed upon the occurrence of protein adsorption, and the physicochemical property of proteins seems to affect the extent of suppression (Figure 3c). Particularly, the binding affinity between proteins and MUTAB−AuNPs is affected by their molecular weight, and the protein with the largest molecular weight (Tf) displays the strongest affinity.

The surface charge also plays a significant role in nano−bio interactions, and previous reports showed that surface net charges of proteins are closely related to their affinity with NPs.[59,60] In a PBS solution with physiological pH (7.0), both BSA and Tf possess the net negative charge, whereas Lyz exhibits the net positive charge (Figure 3c). In the presence of MUTAB−NPs with abundant positive charges, these proteins could adsorb to their surfaces through the anionic patches via electrostatic interactions, and more anionic patches resulted in greater inhibition of the nanozyme activity. BSA and Tf possess more anionic patches and decrease the enzyme-like activity of AuNPs by up to 80%, while Lyz with fewer anionic patches reduced only by 30%.

While these above results demonstrated the feasibility of investigating interactions of AuNPs with the individual protein

https://doi.org/10.1021/acs.analchem.2c01618
Anal. Chem. 2022, 94, 8783−8791

via the proposed approach, it would be more important to testify its suitability in a more biologically relevant medium, plasma serum, which contains hundreds of different proteins and other small molecules. Therefore, we next investigated interactions between these cationic MUTAB−AuNPs and the serum by the present microplate reader-based colorimetric method. As shown in Figure 3d, with increasing the serum concentration, the color of the assay solution gradually faded as in the case of an individual protein, suggesting the inhibition of nanozyme activity owing to the adsorption of serum proteins. Further quantitative analysis could also give the parameter of NP−serum interactions, K_D' = (260 ± 10) × 10^{-8} g/mL (Table 1). Importantly, these results could all be achieved in a multiwell plate simply and rapidly (within 2 h), demonstrating the feasibility and universality of the present colorimetric method for high-throughput quantifying NP−protein interactions.

Table 1. Parameters of Proteins Binding to MUTAB−AuNPs Upon Fitting with the Modified Hill Equation, as Measured by the Microplate Reader

protein	AuNPs	K_D' (10^{-8} M)	E_{max}	n
BSA	AuNPs-5	3.1 ± 0.3	0.87 ± 0.01	0.96 ± 0.08
	AuNPs-10	1.6 ± 0.2	0.87 ± 0.02	0.86 ± 0.04
	AuNPs-15	0.8 ± 0.1	0.72 ± 0.01	0.86 ± 0.10
Tf	AuNPs-5	1.2 ± 0.3	0.79 ± 0.05	0.82 ± 0.12
	AuNPs-10	0.8 ± 0.1	0.86 ± 0.02	0.94 ± 0.10
	AuNPs-15	0.6 ± 0.1	0.73 ± 0.02	0.87 ± 0.01
Lyz	AuNPs-5	131 ± 17	0.34 ± 0.01	0.99 ± 0.11
serum	AuNPs-5	260 ± 10[a]	0.76 ± 0.01	1.05 ± 0.06

[a]Asterisk indicates that the unit is 10^{-8} g/mL.

3.4. Colorimetric Analysis of the Size Effect on Protein−AuNP Interactions. Due to the surface curvature effect, NPs' size has been considered an essential parameter affecting the formation of the protein corona.[61,62] Despite previous studies on NP−bio interactions, the size effect on the protein interactions of cationic NPs remains poorly exploited. Herein, by employing the colorimetry-based approach, we further investigated the influence of NP size on the protein adsorption of MUTAB−AuNPs. We note that for all three MUTAB−AuNPs, their surface charge turned from positive to negative upon incubation with BSA, confirming the occurrence of protein adsorption (Figure S6). We then studied the peroxidase-like activity of MUTAB−AuNPs-10 and MUTAB−AuNPs-15 and optimized the concentration of TMB and H_2O_2 (Figure S7). Interactions between BSA and MUTAB−AuNPs with both sizes were then carried out in microwell plates and compared with the data of AuNPs-5 (Figure 2d). As shown in Figure 4a, it is apparent that the binding of AuNPs to BSA exhibits a strong size-dependent behavior. The obtained parameters such as K_D' (the dissociation constant) and E_{max} (the maximum suppression efficiency) are summarized in Table 1. The results showed that MUTAB−AuNPs with smaller size exhibit larger K_D', suggesting a weaker binding affinity to the surface of BSA (Figure 4b). Similarly, interactions between Tf and MUTAB−AuNPs also exhibit size-dependent behaviors, as shown in Figure 4c,d. Actually, previous studies on the protein adsorption of citrate−AuNPs showed that the binding affinity increases progressively in a particle size range from 5 to 60 nm,[19] and the decrease in K_D' for NPs with enlarged size was also observed in the molecular interaction of poly(acrylic acid)−AuNPs and fibrinogen.[63] On the one hand, the protein packing density on a relatively flat surface of large particles is typically higher than that on the curved surface of small particles.[55] On the other hand, proteins on the surface of NPs with different surface curvatures tend to adopt different conformations, leading to differences in the binding mode and affinity.[64,65]

Upon the protein adsorption, the hydrodynamic sizes of MUTAB−AuNPs were significantly increased as expected. The maximum size increase of both AuNPs-10 and AuNPs-15 upon BSA adsorption is 7.6 and 7.9 nm, respectively, which is approximately the thickness of the monolayer protein corona expected for BSA (Figure S8). This observation is in good agreement with previous studies that the monolayer protein corona will form on the surface of large NPs.[66,67] In stark contrast, the maximum size increase of AuNPs-5 with the smallest size is 26.1 nm, which is much larger than the thickness of the monolayer protein layer expected for BSA. Such a large size increase indicates the occurrence of forming AuNP−protein aggregates, which has also been observed previously for other small NPs.[63,68] The hydrodynamic diameters of ultrasmall NPs are commensurate with those of small- or medium-sized globular proteins, which give rise to protein binding through a more restricted contacting interface compared with that of larger NPs. Consequently, this limited binding interface leads to the formation of small NP−protein complexes with relatively low thermodynamic stability.[69,70] Particularly for cationic NPs, their abundant positive charges easily trigger the assembly of serum proteins that are mostly negatively charged in the physiological pH via strong electrostatic interactions, as seen in the present study. Taken together, the size of these cationic NPs can significantly influence their interactions with proteins, as evidenced by both colorimetric analysis and hydrodynamic size measurement. While MUTAB−AuNPs with the smallest size possess the weakest binding affinity to serum proteins, they tend to form NP−protein complexes owing to their ultrahigh surface curvature (Figure 4e). In contrast, MUTAB−AuNPs with a larger size will form a stable corona layer on their surfaces. These findings provide important implications for the development of these cationic NPs for their potential biomedical applications.

4. CONCLUSIONS

In summary, we presented a colorimetric-based platform for studying protein adsorption onto NPs with enzyme-like activity. Utilizing the peroxidase-like activity of cationic MUTAB−AuNPs, we demonstrated that the colorimetric method is capable of evaluating NP−protein interactions in a simple and high-throughput manner in multiwell plates. Based on quantitative analysis of colorimetric data, we observed that the binding affinity and nanozyme activity inhibition efficiency of MUTAB−AuNPs are strongly influenced by the features of proteins. The inhibition of the nanozyme activity can be considered akin to natural enzymes where proteins bind to their active site and lead to the distinct loss of their catalytic activity. Moreover, the investigation of proteins interacting with MUTAB−AuNPs of different sizes by this colorimetric method underlies the distinct role of particle size in defining the characteristics of the protein adsorption process. Although we focus on the case of cationic AuNPs in this work, one can envision that the protein adsorption onto a variety of other NPs could be investigated by colorimetry similarly. Moreover,

https://doi.org/10.1021/acs.analchem.2c01618
Anal. Chem. 2022, 94, 8783−8791

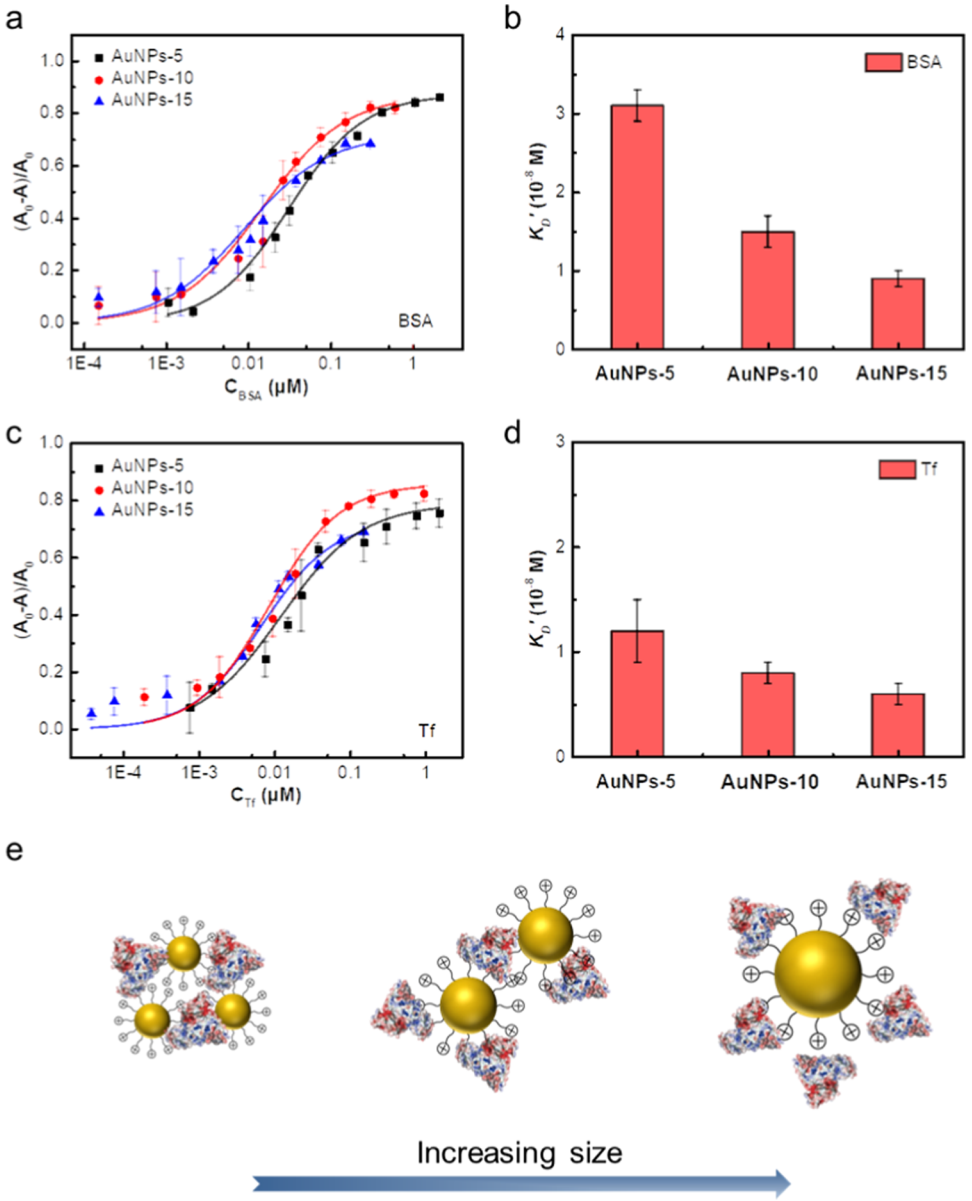

Figure 4. Peroxidase-like activity of MUTAB−AuNPs of different sizes in the presence of BSA (a) or Tf (c) in the TMB−H_2O_2 system. Data were fit to the Hill equation (solid line). (b) and (d) Results of the dissociation coefficients obtained from data in (a) and (c), respectively. (e) Schematic illustration of the interactions between proteins and MUTAB−AuNPs with different sizes. A and A_0 are the absorbances of the solution at 652 nm in the presence and the absence of protein, respectively.

these findings on the protein adsorption on cationic AuNPs would deepen our understanding of their distinct biological behaviors, which will help researchers to design efficient and biocompatible NPs for various biomedical applications.

■ ASSOCIATED CONTENT

Supporting Information

The Supporting Information is available free of charge at https://pubs.acs.org/doi/10.1021/acs.analchem.2c01618.

Details of materials, instrumentation for characterization, synthesis and characterization of MUTAB−AuNPs, TEM images of MUTAB−AuNPs, absorption spectra of the AuNPs-5-catalyzed TMB−H_2O_2 system, circular dichroism spectra of BSA with TMB or H_2O_2, absorption spectra of the BSA−AuNP solution in the presence of TMB or H_2O_2, fluorescence emission spectra of the terephthalic acid probe with AuNPs-5 and BSA, ζ-potential of AuNPs with or without BSA, peroxidase-like activity of AuNPs-10 and AuNPs-15, and hydrodynamic diameters of AuNPs with or without BSA (PDF)

■ AUTHOR INFORMATION

Corresponding Author

Li Shang − *State Key Laboratory of Solidification Processing, School of Materials Science and Engineering, Northwestern Polytechnical University and Shaanxi Joint Laboratory of Graphene (NPU), Xi'an 710072, China;* orcid.org/0000-0003-1575-1934; Email: li.shang@nwpu.edu.cn

Authors

Mengyao Wen − *State Key Laboratory of Solidification Processing, School of Materials Science and Engineering,*

https://doi.org/10.1021/acs.analchem.2c01618
Anal. Chem. 2022, 94, 8783−8791

Northwestern Polytechnical University and Shaanxi Joint Laboratory of Graphene (NPU), Xi'an 710072, China

Juanmin Li − *State Key Laboratory of Solidification Processing, School of Materials Science and Engineering, Northwestern Polytechnical University and Shaanxi Joint Laboratory of Graphene (NPU), Xi'an 710072, China*

Wencheng Zhong − *State Key Laboratory of Solidification Processing, School of Materials Science and Engineering, Northwestern Polytechnical University and Shaanxi Joint Laboratory of Graphene (NPU), Xi'an 710072, China*

Jie Xu − *State Key Laboratory of Solidification Processing, School of Materials Science and Engineering, Northwestern Polytechnical University and Shaanxi Joint Laboratory of Graphene (NPU), Xi'an 710072, China*

Shaohua Qu − *State Key Laboratory of Solidification Processing, School of Materials Science and Engineering, Northwestern Polytechnical University and Shaanxi Joint Laboratory of Graphene (NPU), Xi'an 710072, China*

Hui Wei − *Department of Biomedical Engineering, College of Engineering and Applied Sciences, Nanjing National Laboratory of Microstructures, Jiangsu Key Laboratory of Artificial Functional Materials, Nanjing University, Nanjing, Jiangsu 210023, China;* orcid.org/0000-0003-0870-7142

Complete contact information is available at: https://pubs.acs.org/10.1021/acs.analchem.2c01618

Author Contributions

M.W. contributed to methodology, investigation, data analysis, and writing—original draft; J.L. contributed to methodology and data analysis; W.Z. contributed to methodology and data analysis; J.X. contributed to the investigation and assisting the experiments; S.Q. contributed to methodology and data analysis; H.W. contributed to data analysis and reviewing the manuscript; and L.S. contributed to conceiving the study, data analysis, and finalizing the manuscript.

Notes

The authors declare no competing financial interest.

■ ACKNOWLEDGMENTS

The authors acknowledge support from the National Youth Talents Programme and the Research Fund of the State Key Laboratory of Solidification Processing (NPU), China (2020-QZ-01).

■ REFERENCES

(1) Poon, W.; Kingston, B. R.; Ouyang, B.; Ngo, W.; Chan, W. C. W. *Nat. Nanotechnol.* **2020**, *15*, 819−829.
(2) Sharifi, M.; Attar, F.; Saboury, A. A.; Akhtari, K.; Hooshmand, N.; Hasan, A.; El-Sayed, M. A.; Falahati, M. *J. Controlled Release* **2019**, *311*−*312*, 170−189.
(3) Welch, E. C.; Powell, J. M.; Clevinger, T. B.; Fairman, A. E.; Shukla, A. *Adv. Funct. Mater.* **2021**, *31*, No. 2104126.
(4) Luo, X.; Liu, J. *Adv. Sci.* **2022**, *9*, No. 2103971.
(5) Zhao, J.; Chen, X.; Ho, K.-H.; Cai, C.; Li, C.-W.; Yang, M.; Yi, C. *Chin. Chem. Lett.* **2021**, *32*, 66−86.
(6) Cedervall, T.; Lynch, I.; Lindman, S.; Berggard, T.; Thulin, E.; Nilsson, H.; Dawson, K. A.; Linse, S. *Proc. Natl. Acad. Sci. U.S.A.* **2007**, *104*, 2050−2055.
(7) Monopoli, M. P.; Åberg, C.; Salvati, A.; Dawson, K. A. *Nat. Nanotechnol.* **2012**, *7*, 779−786.
(8) Oh, J. Y.; Kim, H. S.; Palanikumar, L.; Go, E. M.; Jana, B.; Park, S. A.; Kim, H. Y.; Kim, K.; Seo, J. K.; Kwak, S. K.; Kim, C.; Kang, S.; Ryu, J. H. *Nat. Commun.* **2018**, *9*, No. 4548.
(9) Cai, R.; Ren, J. Y.; Ji, Y. L.; Wang, Y. L.; Liu, Y.; Chen, Z. Q.; Sabet, Z. F.; Wu, X. C.; Lynch, I.; Chen, C. Y. *ACS Appl. Mater. Interfaces* **2020**, *12*, 1997−2008.
(10) Francia, V.; Yang, K.; Deville, S.; Reker-Smit, C.; Nelissen, I.; Salvati, A. *ACS Nano* **2019**, *13*, 11107−11121.
(11) Barbalinardo, M.; Bertacchini, J.; Bergamini, L.; Magarò, M. S.; Ortolani, L.; Sanson, A.; Palumbo, C.; Cavallini, M.; Gentili, D. *Nanoscale* **2021**, *13*, 14119−14129.
(12) Cai, R.; Chen, C. Y. *Adv. Mater.* **2019**, *31*, No. 1805740.
(13) Liu, Y.; Wang, J.; Xiong, Q.; Hornburg, D.; Tao, W.; Farokhzad, O. C. *Acc. Chem. Res.* **2021**, *54*, 291−301.
(14) Lundqvist, M.; Cedervall, T. *Small* **2020**, *16*, No. 2000892.
(15) Ma, Y.; Hong, J.; Ding, Y. *Adv. Healthcare Mater.* **2020**, *9*, No. 1901448.
(16) O'Connell, D. J.; Bombelli, F. B.; Pitek, A. S.; Monopoli, M. P.; Cahill, D. J.; Dawson, K. A. *Nanoscale* **2015**, *7*, 15268−15276.
(17) Fernández-Iglesias, N.; Bettmer, J. *Nanoscale* **2015**, *7*, 14324−14331.
(18) Wang, L.; Li, J.; Pan, J.; Jiang, X.; Ji, Y.; Li, Y.; Qu, Y.; Zhao, Y.; Wu, X.; Chen, C. *J. Am. Chem. Soc.* **2013**, *135*, 17359−68.
(19) Lacerda, S. H. D. P.; Park, J. J.; Meuse, C.; Pristinski, D.; Becker, M. L.; Karim, A.; Douglas, J. F. *ACS Nano* **2010**, *4*, 365−379.
(20) Wen, M.; Li, Y.; Zhong, W.; Li, Q.; Cao, L.; Tan, L. L.; Shang, L. *J. Colloid Interface Sci.* **2022**, *610*, 116−125.
(21) Shang, L.; Nienhaus, G. U. *Acc. Chem. Res.* **2017**, *50*, 387−395.
(22) Prozeller, D.; Morsbach, S.; Landfester, K. *Nanoscale* **2019**, *11*, 19265−19273.
(23) Xu, J. X.; Alom, M. S.; Fitzkee, N. C. *Anal. Chem.* **2021**, *93*, 11982−11990.
(24) Weerathunge, P.; Ramanathan, R.; Shukla, R.; Sharma, T. K.; Bansal, V. *Anal. Chem.* **2014**, *86*, 11937−11941.
(25) Zhu, X.; Mao, X.; Wang, Z.; Feng, C.; Chen, G.; Li, G. *Nano Res.* **2017**, *10*, 959−970.
(26) Rao, H.; Xue, X.; Luo, M.; Liu, H.; Xue, Z. *Chin. Chem. Lett.* **2021**, *32*, 25−32.
(27) Tang, G.; He, J.; Liu, J.; Yan, X.; Fan, K. *Exploration* **2021**, *1*, 75−89.
(28) Gao, L.; Zhuang, J.; Nie, L.; Zhang, J.; Zhang, Y.; Gu, N.; Wang, T.; Feng, J.; Yang, D.; Perrett, S.; Yan, X. *Nat. Nanotechnol.* **2007**, *2*, 577−583.
(29) Jv, Y.; Li, B.; Cao, R. *Chem. Commun.* **2010**, *46*, 8017−8019.
(30) Sun, F.; Liang, Y.; Jin, L.; Shi, J.; Shang, L. *ACS Appl. Mater. Interfaces* **2021**, *13*, 58209−58219.
(31) Song, Y.; Qu, K.; Zhao, C.; Ren, J.; Qu, X. *Adv. Mater.* **2010**, *22*, 2206−2210.
(32) Raineri, M.; Winkler, E. L.; Torres, T. E.; Mansilla, V. M.; Nadal, M. S.; Zysler, R. D.; Lima, E. *Nanoscale* **2019**, *11*, 18393−18406.
(33) McVey, C.; Logan, N.; Thanh, N. T. K.; Elliott, C.; Cao, C. *Nano Res.* **2019**, *12*, 509−516.
(34) Liu, B.; Liu, J. *Nano Res.* **2017**, *10*, 1125−1148.
(35) Zhang, R.; Yan, X.; Fan, K. *Acc. Mater. Res.* **2021**, *2*, 534−547.
(36) Li, J. M.; Xu, J.; Guo, W. F.; Zhong, W.; Li, Q.; Tan, L.; Shang, L. *Sens. Actuators, B* **2020**, *305*, No. 127422.
(37) Dragoman, R. M.; Grogg, M.; Bodnarchuk, M. I.; Tiefenboeck, P.; Hilvert, D.; Dirin, D. N.; Kovalenko, M. V. *Chem. Mater.* **2017**, *29*, 9416−9428.
(38) Ewert, K. K.; Scodeller, P.; Simon-Gracia, L.; Steffes, V. M.; Wonder, E. A.; Teesalu, T.; Safinya, C. R. *Pharmaceutics* **2021**, *13*, No. 1365.
(39) Zhan, L.; Li, C.-M.; Gao, P.-F.; Huang, C.-Z. *J. Anal. Test.* **2021**, *5*, 203−209.
(40) Gong, L.; Chen, Y.; He, K.; Liu, J. *ACS Nano* **2019**, *13*, 1893−1899.
(41) Liu, D.; Liu, L.; Liu, F.; Zhang, M.; Wei, P.; Yi, T. *Adv. Sci.* **2021**, *8*, No. e2100074.
(42) Hassinen, J.; Liljestrom, V.; Kostiainen, M. A.; Ras, R. H. *Angew. Chem., Int. Ed.* **2015**, *54*, 7990−7993.

(43) Jana, N. R.; Gearheart, L.; Murphy, C. J. *Langmuir* **2001**, *17*, 6782−6786.
(44) Frens, G. *Nat. Phys. Sci.* **1973**, *241*, 20−22.
(45) Casals, E.; Pfaller, T.; Duschl, A.; Oostingh, G. J.; Puntes, V. *ACS Nano* **2010**, *4*, 3623−3632.
(46) Shang, L.; Dörlich, R. M.; Trouillet, V.; Bruns, M.; Nienhaus, G. U. *Nano Res.* **2012**, *5*, 531−542.
(47) Wang, X. Y.; Wang, X. F.; Wang, M. Z.; Zhang, D.; Yang, Q.; Liu, T.; Lei, R.; Zhu, S. F.; Zhao, Y. L.; Chen, C. Y. *Small* **2018**, *14*, No. 1703982.
(48) Ding, X.; Duan, S.; Ding, X.; Liu, R.; Xu, F.-J. *Adv. Funct. Mater.* **2018**, *28*, No. 1802140.
(49) Li, X.; Wen, F.; Creran, B.; Jeong, Y.; Zhang, X.; Rotello, V. M. *Small* **2012**, *8*, 3589−3592.
(50) Zhang, X.; Liu, Y.; Gopalakrishnan, S.; Castellanos-Garcia, L.; Li, G.; Malassiné, M.; Uddin, I.; Huang, R.; Luther, D. C.; Vachet, R. W.; Rotello, V. M. *ACS Nano* **2020**, *14*, 4767−4773.
(51) Wang, M.; Siddiqui, G.; Gustafsson, O. J. R.; Kakinen, A.; Javed, I.; Voelcker, N. H.; Creek, D. J.; Ke, P. C.; Davis, T. P. *Small* **2017**, *13*, No. 1701528.
(52) Cui, M.; Liu, R.; Deng, Z.; Ge, G.; Liu, Y.; Xie, L. *Nano Res.* **2014**, *7*, 345−352.
(53) Bekdemir, A.; Stellacci, F. *Nat. Commun.* **2016**, *7*, No. 13121.
(54) Canoa, P.; Simon-Vazquez, R.; Popplewell, J.; Gonzalez-Fernandez, A. *Biosens. Bioelectron.* **2015**, *74*, 376−383.
(55) Mishra, K.; Das, P. K. *Phys. Chem. Chem. Phys.* **2019**, *21*, 7675−7684.
(56) Singh, M.; Weerathunge, P.; Liyanage, P. D.; Mayes, E.; Ramanathan, R.; Bansal, V. *Langmuir* **2017**, *33*, 10006−10015.
(57) Liu, Y.; Xiang, Y.; Zhen, Y.; Guo, R. *Langmuir* **2017**, *33*, 6372−6381.
(58) Mo, W. C.; Yu, J.; Gao, L. Z.; Liu, Y.; Wei, Y.; He, R. Q. *Front. Chem.* **2020**, *8*, No. 491.
(59) Shang, L.; Yang, L. X.; Seiter, J.; Heinle, M.; Brenner-Weiss, G.; Gerthsen, D.; Nienhaus, G. U. *Adv. Mater. Interfaces* **2014**, *1*, No. 1300079.
(60) Fleischer, C. C.; Payne, C. K. *J. Phys. Chem. B* **2012**, *116*, 8901−8907.
(61) Gao, G. B.; Zhang, M. X.; Gong, D. J.; Chen, R.; Hu, X. J.; Sun, T. L. *Nanoscale* **2017**, *9*, 4107−4113.
(62) Dobrovolskaia, M. A.; Patri, A. K.; Zheng, J.; Clogston, J. D.; Ayub, N.; Aggarwal, P.; Neun, B. W.; Hall, J. B.; McNeil, S. E. *Nanomedicine* **2009**, *5*, 106−117.
(63) Deng, Z. J.; Liang, M.; Toth, I.; Monteiro, M. J.; Minchin, R. F. *ACS Nano* **2012**, *6*, 8962−8969.
(64) Zhang, X. N.; Zhang, J. T.; Zhang, F.; Yu, S. N. *Nanoscale* **2017**, *9*, 4787−4792.
(65) Deng, J.; Sun, M. C.; Zhu, J. Y.; Gao, C. Y. *Nanoscale* **2013**, *5*, 8130−8137.
(66) Röcker, C.; Pötzl, M.; Zhang, F.; Parak, W. J.; Nienhaus, G. U. *Nat. Nanotechnol.* **2009**, *4*, 577−580.
(67) Wang, H. X.; Ma, R.; Nienhaus, K.; Nienhaus, G. U. *Small* **2019**, *15*, No. 1900974.
(68) Yin, M. M.; Chen, W. Q.; Lu, Y. Q.; Han, J. Y.; Liu, Y.; Jiang, F. L. *Nanoscale* **2020**, *12*, 4573−4585.
(69) Sousa, A. A.; Schuck, P.; Hassan, S. A. *Nanoscale Adv.* **2021**, *3*, 2995−3027.
(70) Kopp, M.; Kollenda, S.; Epple, M. *Acc. Chem. Res.* **2017**, *50*, 1383−1390.

https://doi.org/10.1021/acs.analchem.2c01618
Anal. Chem. 2022, 94, 8783−8791